Biophysical *Journal*
Biophysical Letter

Biophysical Society

Imaging ATP Consumption in Resting Skeletal Muscle: One Molecule at a Time

Shane R. Nelson,[1] Amy Li,[1] Samantha Beck-Previs,[1] Guy G. Kennedy,[1,2] and David M. Warshaw[1,*]
[1]Department of Molecular Physiology and Biophysics, Larner College of Medicine and [2]Instrumentation and Model Facility, University of Vermont, Burlington, Vermont

ABSTRACT Striated muscle contraction is the result of sarcomeres, the basic contractile unit, shortening because of hydrolysis of adenosine triphosphate (ATP) by myosin molecular motors. In noncontracting, "relaxed" muscle, myosin still hydrolyzes ATP slowly, contributing to the muscle's overall resting metabolic rate. Furthermore, when relaxed, myosin partition into two kinetically distinct subpopulations: a faster-hydrolyzing "relaxed" population, and a slower-hydrolyzing "super relaxed" (SRX) population. How these two myosin subpopulations are spatially arranged in the sarcomere is unclear, although it has been proposed that myosin-binding protein C (MyBP-C) may stabilize the SRX state. Because MyBP-C is found only in a distinct region of the sarcomere, i.e., the C-zone, are SRX myosin similarly colocalized in the C-zone? Here, we imaged the binding lifetime and location (38-nm resolution) of single, fluorescently labeled boron-dipyrromethene-labeled ATP molecules in relaxed skeletal muscle sarcomeres from rat soleus. The lifetime distribution of fluorescent ATP-binding events was well fitted as an admixture of two subpopulations with time constants of 26 $\pm$ 2 and 146 $\pm$ 16 s, with the longer-lived population being 28 $\pm$ 4% of the total. These values agree with reported kinetics from bulk studies of skeletal muscle for the relaxed and SRX subpopulations, respectively. Subsarcomeric localization of these events revealed that SRX-nucleotide-binding events are fivefold more frequent in the C-zone (where MyBP-C exists) than in flanking regions devoid of MyBP-C. Treatment with the small molecule myosin inhibitor, mavacamten, caused no change in SRX event frequency in the C-zone but increased their frequency fivefold outside the C-zone, indicating that all myosin are in a dynamic equilibrium between the relaxed and SRX states. With SRX myosin found predominantly in the C-zone, these data suggest that MyBP-C may stabilize and possibly regulate the SRX state.

SIGNIFICANCE Muscle contraction is driven by sarcomere shortening and powered by myosin molecular motors that hydrolyze adenosine triphosphate (ATP). However, myosin in relaxed muscle continues to slowly hydrolyze ATP, analogous to an idling engine. Utilizing superresolution microscopy to directly image single-molecule-fluorescent ATP turnover in relaxed skeletal muscle sarcomeres, we observed two rates of myosin ATP consumption that differed fivefold. These distinct hydrolysis rates were spatially segregated, with the slower or "super relaxed" rate localized predominantly to the sarcomere C-zone. Because myosin-binding protein C, a known modulator of muscle contractile function, is found only in the C-zone, it may also serve to sequester myosin motors into the super relaxed state and thus regulate resting muscle metabolism and force generation upon activation.

In skeletal muscle's most basic contractile unit, the sarcomere (Fig. 1, *A* and *B*), force and motion are generated by "active" myosin molecular motors of the thick filament cyclically interacting with actin thin filaments. To power this contractile process, myosin motors hydrolyze adenosine triphosphate (ATP) (Fig. 1 *E*), with some of the chemical energy lost as heat. Under noncontracting or "relaxed" conditions, myosin is prevented from interacting with actin because of the presence of calcium-dependent regulatory proteins on the thin filament (Fig. 1 *D*). Even when muscle is relaxed, the myosin motors continue to hydrolyze ATP but at a rate two to three orders of magnitude slower than during contraction (1), analogous to the consumption of fuel by an idling car. Because skeletal muscle composes ~40% of an adult human's mass, muscle's energy expenditure and heat generated while relaxed are major contributors to an individual's resting metabolic rate and thermogenesis.

Curiously, myosin's basal ATPase rate in the absence of actin is fivefold greater in vitro than measured in muscle fibers (2), implying an additional inhibitory mechanism

Submitted June 22, 2020, and accepted for publication July 20, 2020.
*Correspondence: david.warshaw@med.uvm.edu
Amy Li's present address is Department of Pharmacy & Biomedical Sciences, La Trobe University, Bendigo, Victoria, Australia.
Editor: Samantha Harris
https://doi.org/10.1016/j.bpj.2020.07.036

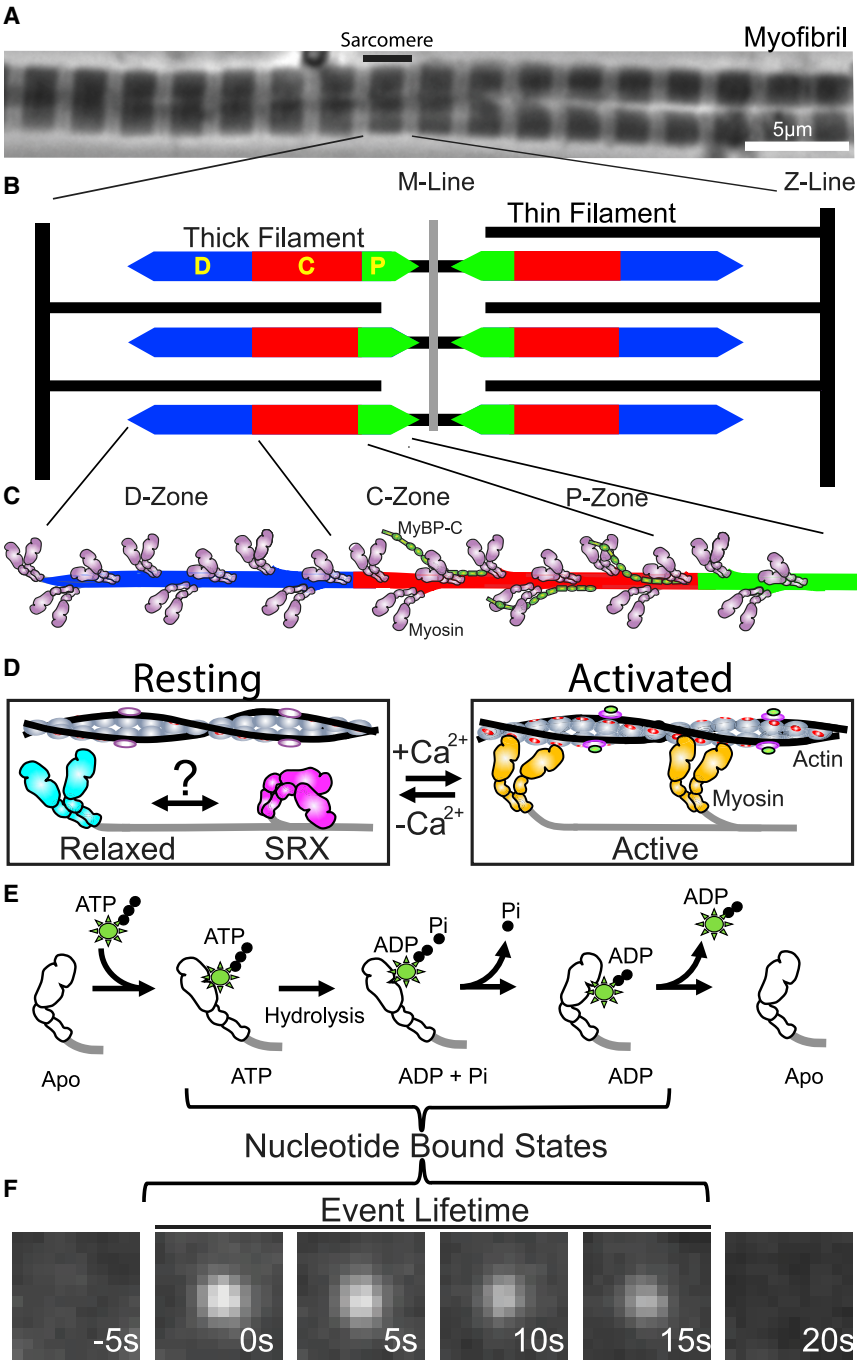

FIGURE 1 Skeletal muscle myofibrils, sarcomeres, and myosin states. (*A*) Phase contrast image of rat soleus myofibrils with sarcomere identified. (*B*) Sarcomere illustration, highlighting interdigitating myosin-based thick filaments and actin-based thin filaments. Thick filaments are bipolar with the M-line at their center. Each thick filament half is described by a D-, C-, and P-zone indicated by different colors. (*C*) Half-thick filament illustration, with myosin motors protruding from the thick filament backbone and MyBP-C only in the C-zone. (*D*) In the resting condition ($-Ca^{2+}$), binding sites on thin filament are blocked by troponin-tropomyosin. Myosin can adopt either a disordered "relaxed" or folded "SRX" state that are in a potential (?) dynamic equilibrium. Under activated conditions ($+Ca^{2+}$), thin filament binding sites are exposed (*red*), and "active" myosin is free to bind actin and cause filament sliding. (*E*) Myosin ATP hydrolysis cycle. Upon binding a fluorescently labeled ATP, the immobilized fluorophore can be visualized as in (*F*). The duration of the observed fluorescence spot is a readout of the total lifetime of the nucleotide bound states. To see this figure in color, go online.

must exist to lower energy usage in relaxed muscle. Thus, recent models, based on muscle fiber ATP consumption, suggest that two myosin populations exist at rest and have kinetically distinct hydrolysis rates: 1) a relaxed myosin population (Fig. 1 *D*), consistent with the previously described in vitro basal rate and 2) a significantly inhibited myosin population, termed "super relaxed" or "SRX" myosin (Fig. 1 *D*; (3)). SRX myosin may represent a "sequestered" or "off" state, which is stabilized by intramolecular interactions formed when myosin molecules in the sarcomere are packed into thick filaments (Fig. 1, *C* and *D*; (4)). Thus, the SRX state may represent a mechanism for conserving energy in relaxed muscle and for regulating force generation in active muscle through sequestration of myosin motors. Is the SRX state itself regulated? Myosin-binding protein C (MyBP-C), a thick filament-associated protein localized to the sarcomere C-zone (Fig. 1, *B* and *C*; (5)), may serve this regulatory role by its proposed stabilization of myosin into the SRX state (6). If so, are SRX myosin similarly limited to the C-zone and not to flanking

regions of the thick filament, which are devoid of MyBP-C (i.e., D- and P-zones; Fig. 1, *B* and *C*)? To address this question, we spatially resolved myosin's hydrolysis of individual fluorescently labeled ATP in relaxed skeletal muscle sarcomeres, allowing us to identify the presence of SRX myosin motors and their location in the thick filament.

Myosin's ATPase rate in the absence of actin is rate limited by the release of its hydrolysis products, inorganic phosphate (P_i), followed by the subsequent release of adenosine diphosphate (ADP) (Fig. 1 *E*; (7)). Thus, fluorescently labeled ATP, in demembranated, relaxed skeletal muscle fibers, was used previously to monitor myosin ATPase rates, either by measuring the uptake of fluorescent ATP or the release of the hydrolysis product, fluorescent ADP (3). By this approach, the myosin SRX state was discovered (3). However, in these large muscle fibers, it was impossible to resolve the spatial location of SRX myosin motors in the sarcomere. Therefore, we isolated myofibrils from slow-twitch, rat soleus muscle. Myofibrils are contractile organelles and consist of long, repeating arrays of sarcomeres that are clearly visible as alternating light and dark bands using phase contrast microscopy (Fig. 1 *A*).

Relaxed myofibrils, adhered to a glass coverslip at room temperature (see Supporting Materials and Methods), were exposed to a limited concentration (10 nM) of fluorescent boron-dipyrromethene-labeled ATP (BODIPY-ATP) and an excess (4 mM) of nonfluorescent ATP, so that 1 out of every 400,000 ATP molecules were fluorescent. This permitted single-molecule imaging of transient fluorescent nucleotide binding in the myofibril (Fig. 1 *F*; Video S1). Because fluorescent-nucleotide-binding events were only seen in myofibrils in which myosin is the predominant ATPase, these events directly report the nucleotide-bound states of myosin's ATPase cycle (Fig. 1, *E* and *F*). Specifically, appearance of a stationary BODIPY-ATP reflects its binding to myosin's apo state, whereas the fluorescence event lifetime encompasses hydrolysis, P_i release, and ultimately the release of BODIPY-ADP (Fig. 1, *E* and *F*). As product release is rate limiting for the hydrolytic cycle, the fluorescence event lifetime (Fig. 1 *F*; *white streaks in kymograph*, Fig. 2 *A*) serves to estimate the myosin ATPase cycle time. The fit to the survival plot of fluorescence event lifetimes ($n = 734$ events from 259 sarcomeres from 20 myofibrils) was best described by the sum of two exponential populations (ATP, Fig. 2 *B*), as shown by reduced residuals from the fits (Fig. 2 *C*). The time constants differ by fivefold (i.e., 26 ± 2 and 146 ± 16 s), with the longer lifetime population accounting for 28 ± 4% of the total (*inset*, Fig. 2 *B*; Table S1). These time constants are in agreement with rabbit soleus fiber-level measurements (3), suggesting the longer lifetime population is reflective of SRX myosin.

Upon muscle activation, SRX myosin must rapidly transition to the "relaxed" state and subsequently to the "active" state (Fig. 1 *D*) to generate force and motion (8).

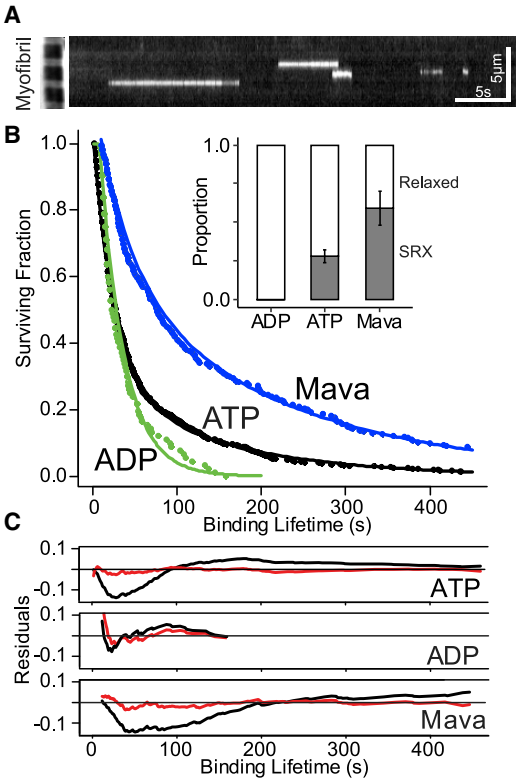

FIGURE 2 Fluorescent-nucleotide-binding lifetimes. (*A*) Kymograph of multiple fluorescent-nucleotide-binding events (individual streaks), with phase contrast image of a myofibril provided (*left side*) for scale. (*B*) Survival plot of fluorescent-nucleotide-binding lifetimes for myofibrils incubated in ADP (*green*), ATP (*black*), or ATP + Mavacamten (Mava) (*blue*). Lines are double exponential fits to each data set and inset shows relative proportions of relaxed (*white*) and SRX (*gray*) events for each experimental condition. Error bars indicate standard error for double exponential fits. (*C*) Residuals from fitting each experimental condition are reduced and lack clear structure when fit with double (*red*) versus single (*black*) exponential. To see this figure in color, go online.

In fact, in experiments in which 4 mM unlabeled ATP was replaced with 4 mM unlabeled ADP so that myosin strong-binding was favored (9), myofibrils were unable to relax, thus preventing myosin from entering the SRX state (3). When these myofibrils were exposed to 10 nM BODIPY-ATP, myofibrils slowly contracted at 0.002 sarcomere lengths/s. Under these nonrelaxing conditions, the fluorescence event lifetimes ($n = 116$ events from 159 sarcomeres from six myofibrils) were best fitted by a single population with lifetimes (i.e., 25 ± 2 s) equal to the shorter lifetimes measured in relaxed myofibrils, with no evidence of SRX myosin (ADP, Fig. 2 *B*; Table S1). The observed kinetics suggest that the long-lived fluorescence lifetimes are sensitive to the myofibril's activation state, as predicted for the SRX state, and not merely an artifact of nonspecific BODIPY-ATP binding. To further support the myosin-specific nature of these events, we used mavacamten: a myosin-selective, small molecule ATPase inhibitor (10) that stabilizes

the myosin SRX state (11). When resting myofibrils were treated with 10 μM mavacamten, the fluorescence lifetime survival plot (n = 246 events from 328 sarcomeres from 31 myofibrils) was once again best fitted by two populations with time constants ~50% longer than in the absence of mavacamten (Mava, Fig. 2 *B*). Additionally, the overall proportion of SRX events doubled from 28 ± 4 to 59 ± 11% (*inset*, Fig. 2 *B*; Table S1), confirming the SRX population originates from myosin and that mavacamten does enhance the presence of the SRX state.

The myofibril's well-defined structure allowed us to spatially localize SRX myosin in the sarcomere and thus determine if SRX myosins are confined to a specific location or distributed throughout the thick filament. Sarcomeres exhibit bilateral, structural symmetry about the M-line at the sarcomere center (Fig. 1 *B*), where myomesin, an Ig-superfamily protein, exists and connects adjacent thick filaments (12). By identifying sarcomere centers through myomesin immunofluorescence (Fig. 3 *A*), the center-to-center distance averaged 2.2 ± 0.2 μm, consistent with sarcomere lengths (2.3 ± 0.1 μm, N = 235 sarcomeres) measured from Z-line to Z-line in phase contrast images of myofibrils (Fig. 1 *A*). Then BODIPY-ATP-binding events and myomesin (M-line) were localized (Fig. 3 *A*) using superresolution detection algorithms (see Supporting Materials and Methods) so that the distance between each BODIPY-ATP-binding event and the M-line was measured with a combined error (σ) of 38 nm. Fluorescence binding events (n = 302 events) appeared randomly distributed up to 971 nm from the M-line (Fig. 3 *B*). With the distance from the M-line to the thick filament end being 817 nm (13) and allowing for localization error (σ), 97% of the BODIPY-ATP-binding events lie in the span of the myosin thick filament, providing further evidence for the myosin-specific nature of these events.

Although no spatial bias was apparent for the BODIPY-ATP-binding events (Fig. 3 *B*), could the long-lived SRX event population be localized to a specific sarcomeric region and thus the thick filament? To address this objectively, we developed a simple "Monte Carlo-style" model that simulated fluorescent-nucleotide-binding events along a half thick filament length (see Supporting Materials and Methods). By comparing experimental data to simulated results, a landscape emerges where the best fit to the

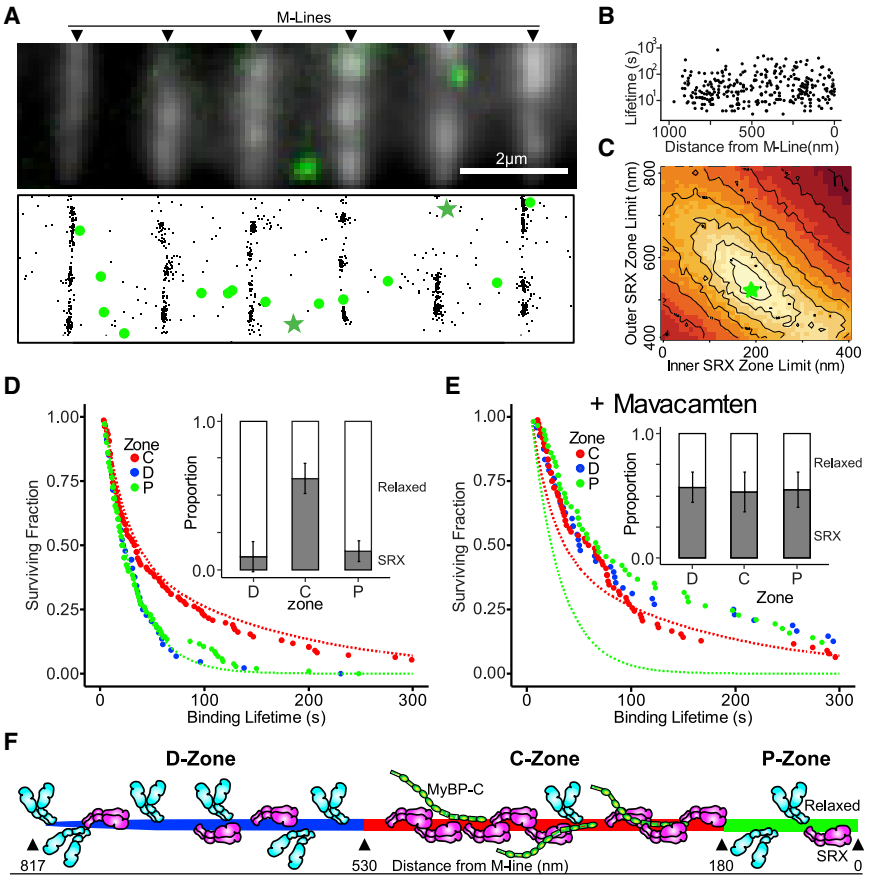

FIGURE 3 Spatial localization of fluorescent-nucleotide-binding events. (*A*) Top panel shows fluorescence image of antimyomesin-labeled (M-line) myofibrils with an overlaid still frame showing two fluorescent-nucleotide-binding events (*larger green spots*). Bottom panel shows color- and drift-corrected subpixel localizations for myomesin (*black points*) and fluorescent-nucleotide events (*green*), with binding events from the upper panel denoted (*green stars*). (*B*) Scatterplot of fluorescent-nucleotide-binding event lifetimes versus distance from nearest M-line. (*C*) Root mean-square deviation heatmap comparing a simulated SRX-containing zone of variable width (i.e., bounded by inner and outer limits) to experimental data (see Supporting Materials and Methods). Lighter colors denote better fits, with best fit (*green star*; SRX Zone Limits: *Inner*, 180 nm; *Outer*, 530 nm). (*D*) Survival plots of binding event lifetimes localized to D-, C-, and P-zones. Dashed lines indicate theoretical curves if a zone contained only relaxed events (*green*) or entirety SRX events (*red*). Inset bar chart shows proportions of relaxed (*white*) and SRX (*gray*) events by zone. Error bars indicate standard error for double exponential fits. (*E*) As in (*D*), but for myofibrils incubated in ATP with Mavacamten. (*F*) Cartoon illustrating that C-zone contains the preponderance of sequestered SRX myosin (*magenta*, *folded*), whereas D- and P-zones contain predominantly relaxed myosin (*cyan*, *extended*). Distances for zones determined by modeling effort in (*C*). To see this figure in color, go online.

experimental data suggests that SRX events occurred between 180 and 530 nm from the M-line (Fig. 3 *C*). This predicted 350 nm SRX-containing zone agrees with the C-zone location we recently reported in rat soleus fibers, based on MyBP-C immunofluorescence (13). Using this model prediction, we parsed the experimentally observed nucleotide binding events into the C-zone (180–530 nm from the M-line, $n = 111$) and its flanking D-zone (>530 nm from the M-line, $n = 125$) and P-zone (<180 nm from the M-line, $n = 66$), which are both devoid of MyBP-C (Fig. 3 *F*). We then fit fluorescence lifetime survival plots for each of these zones to double exponentials (Fig. 3 *D*). Based on these fits, the C-zone had 61 ± 12% SRX events, whereas the flanking D- and P-zones had 9 ± 12 and 13 ± 8% SRX, respectively (Fig. 3 *D*; Table S1). Thus, the SRX state appears enriched in the C-zone. However, as the slower SRX myosin population cycles through approximately fivefold less ATP in the same time as the faster "relaxed" myosin population, the SRX proportion of observed fluorescent-nucleotide-binding events (Figs. 2 *B* and 3, *D* and *E*), must underestimate the true SRX myosin population. Therefore, we developed a simple model (see Supporting Material) to account for this discrepancy, wherein the observed frequency of fluorescent-nucleotide-binding events is a function of both the underlying proportion of the myosin populations (relaxed or SRX), as well as the ratio of those populations' hydrolytic rates. Using this model, we estimate that 89% of myosin in the C-zone are in the SRX state, compared to ~40% in each of the D- and P-zones (Table S1) as illustrated in Fig. 3 *F*. Across the entire sarcomere, we estimate that 68% of myosin is in the SRX state, which is in close agreement with the 56% reported in prior skinned fiber studies (3).

When myofibrils were treated with 10 μM mavacamten, the proportion of SRX events doubled (Fig. 2 *B*; Table S1). So, where along the thick filament length did the increased SRX population originate? When BODIPY-ATP-binding events ($n = 246$ from 222 sarcomeres and 20 myofibrils) were spatially mapped by their distance from the M-line, the proportion of SRX events in the C-zone (53 ± 12%) was not significantly different compared to untreated myofibrils ($p > 0.05$, Table S1). However, the events in the D- and P-zones demonstrated a marked shift toward the SRX state (Fig. 3, *D* and *E*; Table S1). In fact, when the ATPase turnover model (see above) was used to calculate the SRX myosin population for the various zones, the D- and P-zones estimates of 88 and 87%, respectively, were nearly equal to the 86% predicted for the C-zone (Table S1), which is visually discernable by comparing the fluorescence lifetime plots in Fig. 3 *D* versus Fig. 3 *E*. Thus, the increased SRX myosin population with mavacamten was restricted to the C-zone flanking regions, confirming that myosin along the entire thick filament length can enter the SRX state. However, without pharmacologic intervention, SRX myosin state are enriched only in the C-zone, supporting MyBP-C's putative role in stabilizing this state.

With the majority of SRX myosin motors being spatially segregated to the C-zone in resting myofibrils, what are the functional implications of this spatial segregation? In skeletal muscle, MyBP-C is believed to be a critical modulator of contractility, with its modulatory effects limited to the C-zone (13), where MyBP-C may sequester myosin into the SRX state. Interestingly, patients with skeletal MyBP-C mutations exhibit distal arthrogryposis, a condition with extreme muscle contractures (14), suggesting an impaired ability of mutant MyBP-C to sequester myosin motors into the SRX state. In fact, mutations in the cardiac isoform of MyBP-C do result in reduced proportions of SRX myosin, which may explain the hypercontractility and impaired relaxation that are characteristic of these cardiomyopathies (15,16). Therefore, focus on MyBP-C as a therapeutic target to modulate muscle metabolism and force generation is warranted.

SUPPORTING MATERIAL

Supporting Material can be found online at https://doi.org/10.1016/j.bpj.2020.07.036.

AUTHOR CONTRIBUTIONS

S.R.N. methodology, software, formal analysis, investigation, resources, writing (original draft, review, and editing), and visualization. A.L. investigation and resources. S.B.-P. investigation and resources. G.G.K. methodology, resources, and visualization. D.M.W. conceptualization, writing (review and editing), supervision, project administration, and funding acquisition. Data and materials availability: all data are available in the manuscript or the Supporting Materials and Methods. Software available upon request.

ACKNOWLEDGMENTS

The authors wish to acknowledge George Osol and Marilynn Cipolla (University of Vermont) for contribution of biological samples and insightful conversations early on with Michael Geeves and Neil Kad (University of Kent).

Funding: National Institutes of Health Grants AR067279, HL126909, and HL150953 (to D.M.W.) and supported in part by a generous gift to D.M.W. from Arnold and Mariel Goran.

REFERENCES

1. Weeds, A. G., and R. S. Taylor. 1975. Separation of subfragment-1 isoenzymes from rabbit skeletal muscle myosin. *Nature.* 257:54–56.
2. Kushmerick, M. J., and R. J. Paul. 1976. Relationship between initial chemical reactions and oxidative recovery metabolism for single isometric contractions of frog sartorius at 0 degrees C. *J. Physiol.* 254:711–727.
3. Stewart, M. A., K. Franks-Skiba, …, R. Cooke. 2010. Myosin ATP turnover rate is a mechanism involved in thermogenesis in resting skeletal muscle fibers. *Proc. Natl. Acad. Sci. USA.* 107:430–435.

4. Alamo, L., A. Pinto, …, R. Padrón. 2018. Lessons from a tarantula: new insights into myosin interacting-heads motif evolution and its implications on disease. *Biophys. Rev.* 10:1465–1477.
5. Bennett, P., R. Craig, …, G. Offer. 1986. The ultrastructural location of C-protein, X-protein and H-protein in rabbit muscle. *J. Muscle Res. Cell Motil.* 7:550–567.
6. McNamara, J. W., A. Li, …, R. Cooke. 2016. Ablation of cardiac myosin binding protein-C disrupts the super-relaxed state of myosin in murine cardiomyocytes. *J. Mol. Cell. Cardiol.* 94:65–71.
7. Kawas, R. F., R. L. Anderson, …, H. M. Rodriguez. 2017. A small-molecule modulator of cardiac myosin acts on multiple stages of the myosin chemomechanical cycle. *J. Biol. Chem.* 292:16571–16577.
8. Cooke, R. 2011. The role of the myosin ATPase activity in adaptive thermogenesis by skeletal muscle. *Biophys. Rev.* 3:33–45.
9. Lymn, R. W., and E. W. Taylor. 1971. Mechanism of adenosine triphosphate hydrolysis by actomyosin. *Biochemistry.* 10:4617–4624.
10. Green, E. M., H. Wakimoto, …, C. E. Seidman. 2016. A small-molecule inhibitor of sarcomere contractility suppresses hypertrophic cardiomyopathy in mice. *Science.* 351:617–621.
11. Anderson, R. L., D. V. Trivedi, …, J. A. Spudich. 2018. Deciphering the super relaxed state of human β-cardiac myosin and the mode of action of mavacamten from myosin molecules to muscle fibers. *Proc. Natl. Acad. Sci. USA.* 115:E8143–E8152.
12. Eppenberger, H. M., J. C. Perriard, …, E. E. Strehler. 1981. The Mr 165,000 M-protein myomesin: a specific protein of cross-striated muscle cells. *J. Cell Biol.* 89:185–193.
13. Li, A., S. R. Nelson, …, D. M. Warshaw. 2019. Skeletal MyBP-C isoforms tune the molecular contractility of divergent skeletal muscle systems. *Proc. Natl. Acad. Sci. USA.* 116:21882–21892.
14. Ha, K., J. G. Buchan, …, C. A. Gurnett. 2013. MYBPC1 mutations impair skeletal muscle function in zebrafish models of arthrogryposis. *Hum. Mol. Genet.* 22:4967–4977.
15. McNamara, J. W., A. Li, …, C. G. Dos Remedios. 2017. MYBPC3 mutations are associated with a reduced super-relaxed state in patients with hypertrophic cardiomyopathy. *PLoS One.* 12:e0180064.
16. Toepfer, C. N., H. Wakimoto, …, C. E. Seidman. 2019. Hypertrophic cardiomyopathy mutations in MYBPC3 dysregulate myosin. *Sci. Transl. Med.* 11:eaat1199.

Biophysical Journal, Volume *119*

Supplemental Information

Imaging ATP Consumption in Resting Skeletal Muscle: One Molecule at a Time

Shane R. Nelson, Amy Li, Samantha Beck-Previs, Guy G. Kennedy, and David M. Warshaw

Materials and Methods

Myofibril Preparation

Glycerinated muscle strips were prepared from soleus muscle from female, non-pregnant Sprague Dawley rats. Muscle strips of approximately 1-2mm diameter and 1.5cm in length were tied to toothpicks using silk sutures and washed in Rigor Buffer (50 mM Tris, 100 mM $Nacl_2$, 2mM KCl, 2mM $MgCl_2$, 10 mM EGTA, 0.5mM DTT, protease inhibitor cocktail, pH 7.4) twice for 12 hours each time, at 4°C. This was followed by two washes (12 hours each) with a 50:50 glycerol: Rigor Buffer, and finally stored at -20°C for a minimum of 7 days in 50:50 glycerol: Rigor Buffer.

Myofibrils were prepared from glycerinated muscle strips immediately prior to imaging by dissecting a thin strip (~1mm diameter) and de-glycerinating by soaking in 1.5ml of Myofibril Preparation Buffer (50 mM Tris, 100 mM KCl, 4mM $MgCl_2$, 2mM EGTA, protease inhibitor cocktail, pH 7.0) on ice for 1 hour. Samples were then mechanically sheared using a "Tissue Tearor" homogenizer (Biospec Products, Bartlesville, OK) according to the following speed ramp (in 1000X RPM): 3-9-15-21-15-9-3, for 5 seconds at each speed. Samples were then allowed to settle on ice for 10-15 minutes.

Imaging Conditions

From the tube of prepared myofibrils, 200µl were drawn from the bottom of the tube and incubated with anti-myomesin antibody (Cat #EPR17322-9, Abcam, Cambridge UK) at a 1:5000 final dilution for 15 minutes on ice, followed by Alexa 647 goat-anti-mouse IgG (Cat #A21237, Life Technologies, Carlsbad CA) at a final concentration of 1:5000. After 5 minutes on ice, labeled myofibrils were flowed into flowcells, prepared as described previously *(1),* which were made using plasma-cleaned glass. The flowcell was then incubated at room temperature for 20 minutes to allow myofibrils to adhere to the coverglass surface. Finally, 100µl of Relaxing Buffer (120mM KOAc, 5mM K-phosphate, 4mM EGTA, 4mM $MgCl_2$, 50mM MOPS, 4mM ATP, 10nM BODIPY-ATP (Cat #A12410, ThermoFisher, Waltham MA), pH 6.8) was flowed into the flowcell and samples were imaged using a custom-built dual camera super-resolution microscope, described previously *(2)* for 50 minutes at 10FPS. From each myofibril preparation 2-4 recordings were made, with each flowcell being used for only a single imaging session.

Image Analysis

BODIPY-ATP binding lifetimes and positions were measured separately to maximize accuracy and precision. Lifetimes were measured manually from kymographs to account for visually apparent blinking behavior, while position information was calculated using ThunderSTORM localizations, along with drift and channel offset corrections. Details below:

BODIPY-ATP binding events (green channel) were manually documented in image stacks using ImageJ *(3).* First, image stacks were integrated to 1FPS using the "grouped Z-project" function. Image stacks were then converted into a stack of kymographs using the "Reslice" function and events were documented using rectangular selections and the "overlay" function. Sub-pixel localizations of both BODIPY-ATP and Myomesin label (red channel) were performed using

ThunderSTORM plugin *(4)*. Finally, BODIPY-ATP binding lifetimes (from kymograph analysis) were connected to sub-pixel localizations, as the kymograph X, Y, and Slice coordinates can be directly related to Timestamp, X, and Y coordinates (respectively) in the ThunderSTORM output files.

Positions of each M-line were calculated by regression of a line segment by adjusting the segment's defining coordinates (X_1, Y_1, X_2, Y_2) to minimize the summed distance squared between each ThunderSTORM localization and the segment. Red channel localizations from only the initial 200 seconds of the recording were used, due to photobleaching, as well as to minimize the blurring effects of stage drift

Drift correction was performed by tracking a fiducial marker (any persistent spot in either red or green channel) over the timecourse of the experiment, followed by linear (occasionally piece-wise) regression to X vs Time and Y vs Time data separately. Coordinates for BODIPY-ATP localizations were then drift corrected by subtracting the calculated drift that occurred between the start of the recording and the onset of each BODIPY-ATP binding event.

Spatial offsets between red and green imaging channels were calculated by imaging multicolor-fluorescent beads (Tetraspeck, ThermoFisher) and analysis using the Particle Image Velocimetry plugin for ImageJ *(5)*, which calculates relative offsets between the two images by maximizing cross-correlation between corresponding regions in the two images.

Finally, coordinates of BODIPY-ATP binding events (green channel) were drift- and color-corrected to pixel coordinates of the Myomesin (red channel) at the start of the recording, and distances were calculated between each binding event and the fitted M-line segment.

Error propagation of the combined error for BODIPY-ATP localization, M-line localization, drift, and channel correction yields an overall estimate of 38nm (S.D.) on measured sub-sarcomeric localizations.

Fluorescent Event Lifetime Fitting

Events < 3s in duration are rarely detected above background in our analysis, therefore, fluorescence event lifetimes were fit with single and double exponential models that account for a lack of the shortest event lifetimes in our experimental distributions:

Single Exponential:

$$f(x;t) = e^{-x/t} / \left(1 - \left(1 - e^{-\min(x)/t}\right)\right)$$

Double Exponential:

$$f(x;P1,t_1,t_2) = \frac{P_1 e^{-\frac{x}{t_1}}}{\left(1 - \left(1 - e^{-\frac{\min(x)}{t_1}}\right)\right)} + \frac{(1-P_1)e^{-x/t_2}}{\left(1 - \left(1 - e^{-\frac{\min(x)}{t_2}}\right)\right)}$$

Where P_1 is the proportion of "relaxed" events, t_1 is the time constant for the relaxed population, and t_2 is the time constant of the SRX population. Lifetimes were fit by direct optimization of the log-likelihood estimates as implemented in the "fitdistr" function included in the "MASS" library for the statistical programming language "R" (*6*) using the "L-BFGS-B" method *(7)*.

Actin Filament Motility to Validate BODIPY-ATP

In vitro motility was performed using myosin and actin purified from Chicken pectoralis muscle *(8)*. Actin was labeled with Alexa 647-phalloidin. Motility experiments were performed as described previously *(1)* at 25, 50, and 100μM ATP or BODIPY-ATP. Movies were recorded at 15FPS on an inverted Nikon DE2000 scope. Three movies were recorded and analyzed per condition, with tracking performed with the "MTrack2" plugin for ImageJ. Velocity vs [ATP] data were fit with a Michaelis-Menten relationship using "Dose-Response Model Fitting" as implemented in the DRM package of the statistical programming language "R" *(6)*. Results shown in Figure S1, demonstrating that BODIPY-ATP sustains myosin activity in a nearly identical manner to ATP, even at very limiting [ATP].

Monte Carlo Simulation

We developed a model to help determine the spatial arrangement of Relaxed and SRX myosin along a half-thick filament without pre-supposing that these myosin states exist within defined P-, C- and D-zone boundaries. Therefore, we compared the experimental nucleotide binding event localizations (Main text, Fig. 3B) with simulated data sets having alternate spatial arrangements of SRX and Relaxed events within the sarcomere. This enabled us to determine whether the experimental data were in better agreement with alternate spatial localization hypotheses (e.g., uniformly distributed, or in other spatially distinct regions along the thick filament). Therefore, we simulated plots of Fluorescence Binding Lifetime vs Distance that would arise if the SRX events occur within a select region of the half-thick filament. Simulations and comparisons to experimental results were performed as follows:

1) Distances of simulated fluorescent nucleotide binding events from the M-line are generated from a uniform distribution between 0 and 817nm (i.e., the half-thick filament length).

2) Individual fluorescent nucleotide binding events (n=300 events), along the entire length of the half-thick filament, are initially populated with "Relaxed" myosin state lifetimes by drawing random numbers from an exponential distribution with a time constant (reciprocal rate) of 26s.

3) The lifetimes of randomly selected events within a select region, bounded by "Inner" and "Outer" limits (Fig. S2A) were replaced with SRX myosin state lifetimes drawn from an exponential distribution with a time constant of 146s. The number of events that were "converted" to SRX events was fixed at 28% of the total number of events, to match the experimentally observed overall SRX event frequency (Table 1; Main text Fig. 2B).

4) The simulated data were compared to the experimental data as follows:

A) Each fluorescence binding event has a measured distance from the M-line, measured in nanometers (termed *M*). The entire event population is then split into "proximal" and "distal" sub-populations by a dividing line (*D*, also measured in nm from the M-line).

B) Each sub-population of events (defined by $M<D$ and $M>D$) is independently fit with the double exponential model (described above).

C) A Ratio of SRX proportions (*R,* as a function of the position of dividing line, *D*) was calculated based on the SRX population in each of two sub-populations according to:

$$R(D) = \frac{P_{SRX,M<D}}{P_{SRX,M>D}}$$

where P_{SRX} is the proportion of SRX events (1-P_1 from the double exponential fit to the fluorescence binding lifetime, see above), over the range of $200<D<650$nm. A plot of R(D) for both simulated (red) and experimental data (black) is shown in Fig. S2B

D) The difference in R(D) profiles for simulated and experimental data were then calculated as the Root Mean Squared Difference (RMSD)

5) The "Inner" bound (from Step 3) was varied in 10nm increments from 0-400nm from the M-line, and the "Outer" bound was varied from 410-810nm in 10nm increments. This allowed for testing of all hypothetical SRX containing zones, up to and including that where SRX events are uniformly distributed across the entire half-thick filament (i.e., bounds of 0 and 810nm, respectively). The RMSD between simulation and experiment as a function of the inner and outer bounds is shown in main text Fig. 3C.

Myosin State Proportions Model

Myofibril experiments were all performed at saturating 4mM ATP. Under these conditions, ATP binding is rapid, such that myosin spends the majority of the time in a nucleotide-bound state. In skinned fiber experiments, *(9),* 96% of myosin are estimated to be bound with ATP under similar conditions reported here. Therefore, the total ATPase cycle time for both "relaxed" and super-relaxed (SRX) myosin should be reflected in our experimentally measured nucleotide-bound lifetimes for these populations. Therefore, during experiments, relaxed myosin molecules should turnover ~5-fold more ATP than SRX myosin. Therefore, we propose a simple model, where the observed "relaxed" event frequency ($P_{1,OBS}$) is related to the proportion of relaxed myosin in the myofibril (P_1) and the fluorescence lifetimes of both relaxed and SRX myosin (T_1 and T_2, respectively):

$$P_{1,OBS} = \frac{P_1/T_1}{(P_1/T_1) + \big((1-P_1)/T_2\big)}$$

The relationship between observed binding events and the underlying myosin proportions are shown in Figure S3.

Supplementary Materials Works Cited

1. Warshaw, D.M., J.M. Desrosiers, S.S. Work, K.M. Trybus. 1990. Smooth muscle myosin cross-bridge interactions modulate actin filament sliding velocity in vitro. J Cell Biol. 111:453–463.

2. Nelson, S.R., S.D. Kathe, T.S. Hilzinger, A.M. Averill, D.M. Warshaw, S.S. Wallace, A.J. Lee. 2019. Single molecule glycosylase studies with engineered 8-oxoguanine DNA damage sites show functional defects of a MUTYH polyposis variant. Nucleic Acids Res. 47:3058-3071 .

3. Schindelin, J., I. Arganda-Carreras, E. Frise. 2012. Fiji: an open-source platform for biological-image analysis, Nature Methods 9, 676-682 (2012).

4. Ovesný, M., P. Křížek, J. Borkovec, Z. Svindrych, G.M. Hagen. 2014. ThunderSTORM: a comprehensive ImageJ plug-in for PALM and STORM data analysis and super-resolution imaging. Bioinformatics. 30:2389–2390.

5. Tseng, Q., E. Duchemin-Pelletier, A. Deshiere, M. Balland, H. Guillou, O. Filhol, M. Théry. 2012. Spatial organization of the extracellular matrix regulates cell-cell junction positioning. Proc Natl Acad Sci U S A.109:1506-1511.

6. Venables, W.N., B.D. Ripley. 2002. Modern Applied Statistics with S. Fourth edition. Springer, New York.

7. Byrd, R.H., P. Lu, J. Nocedal, C. Zhu. 1995. A limited memory algorithm for bound constrained optimization. SIAM Journal on Scientific Computing. 16:1190–1208.

8. Pardee, J.D., J.A. Spudich. 1982. Purification of muscle actin. Methods Cell Biol. 24:271-289.

9. Stewart, M.A., K. Franks-Skiba, S. Chen, R. Cooke. 2010. Myosin ATP turnover rate is a mechanism involved in thermogenesis in resting skeletal muscle fibers. Proc. Nat. Acad. Sci. U.S.A. 107: 430-435.

	Nucleotide Binding Events						Modeled Myosin Proportions	
Condition	**SRX Proportion**	**T1 (sec)**	**T2 (sec)**	**Events (N)**	**Myofibrils (N)**	**Sarcomeres (N)**	**Relaxed**	**SRX**
ATP Overall	0.28±0.04	25.92±2.10	145.6±15.7	734	20	259	0.33	0.67
C-Zone	0.61±0.12	20.95±6.10	153.1±31.6	111	9	120	0.11	0.89
D-Zone	0.09±0.12	27.88±6.76	151.8±89.8	125	9	120	0.64	0.36
P-Zone	0.13±0.08	24.45±4.77	149.8±88.0	66	9	120	0.54	0.46
ADP Overall		24.63±2.29		116	16	159		
Mava Overall	0.59±0.11	41.90±11.20	198.0±29.6	246	31	328	0.11	0.89
C-zone Mava	0.53±0.12	40.55±8.67	197.6±44.3	80	20	222	0.14	0.86
D-Zone Mava	0.57±0.16	35.10±15.93	208.0±42.0	67	20	222	0.12	0.88
P-Zone Mava	0.55±0.14	28.60±9.74	204.4±47.5	49	20	222	0.13	0.87

Table S1. Fluorescent-Nucleotide Binding Events and Modeled Myosin Proportions. "SRX Proportion" is the proportion of events attributable to the SRX population, "T1" and "T2" are time constants for the "relaxed" and SRX populations, respectively, from fitting event lifetime data with double exponential model, ± values are estimated standard errors of the fit (see Supplementary Materials), N is the number of total events, myofibrils or sarcomeres. Modeled Myosin Proportions are calculated based upon the "Myosin State Proportions Model," details in Supplementary Materials. "Mava" denotes myofibrils treated with Mavacamten.

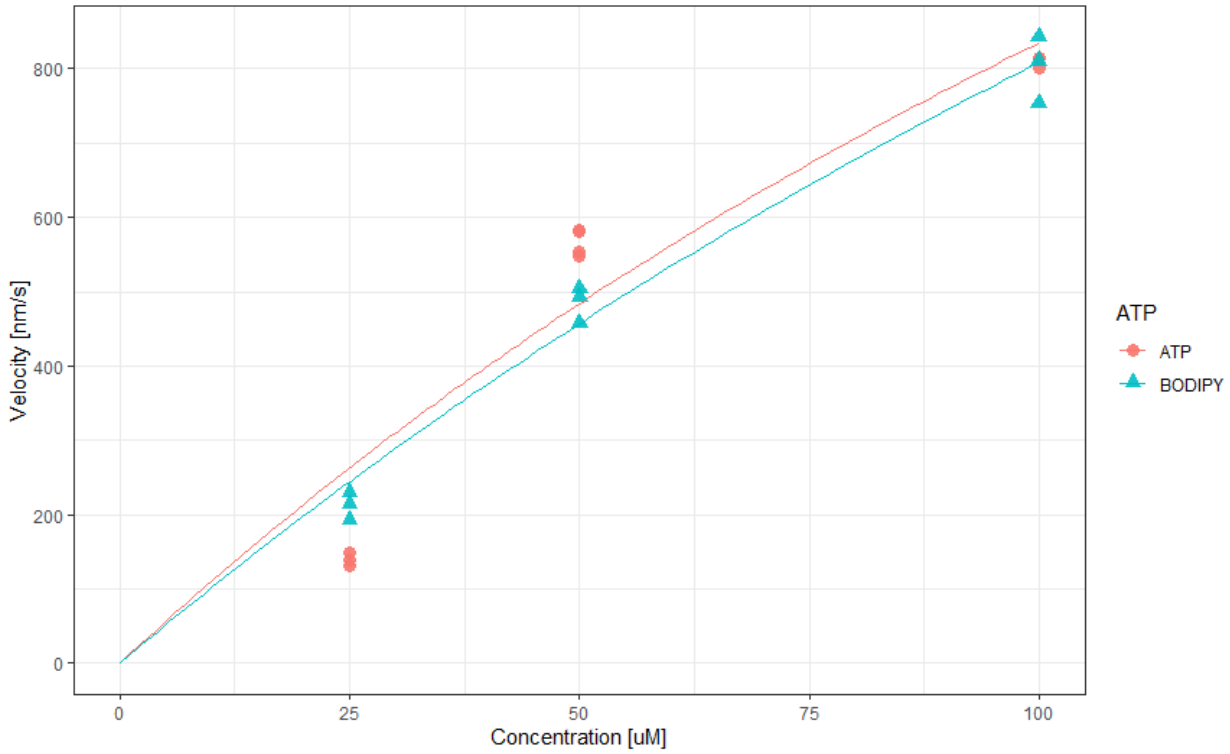

Figure S1. Velocity in gliding filament motility assay as a function of concentration of unlabeled ATP and fluorescent BODIPY-ATP. Fitted Values are: V_{max}: 3.03±1.82µm/s and K_m: 264±204µM for unlabeled ATP and V_{max}: 3.49±1.24µm/s and K_m: 332±147µM for BODIPY-ATP.

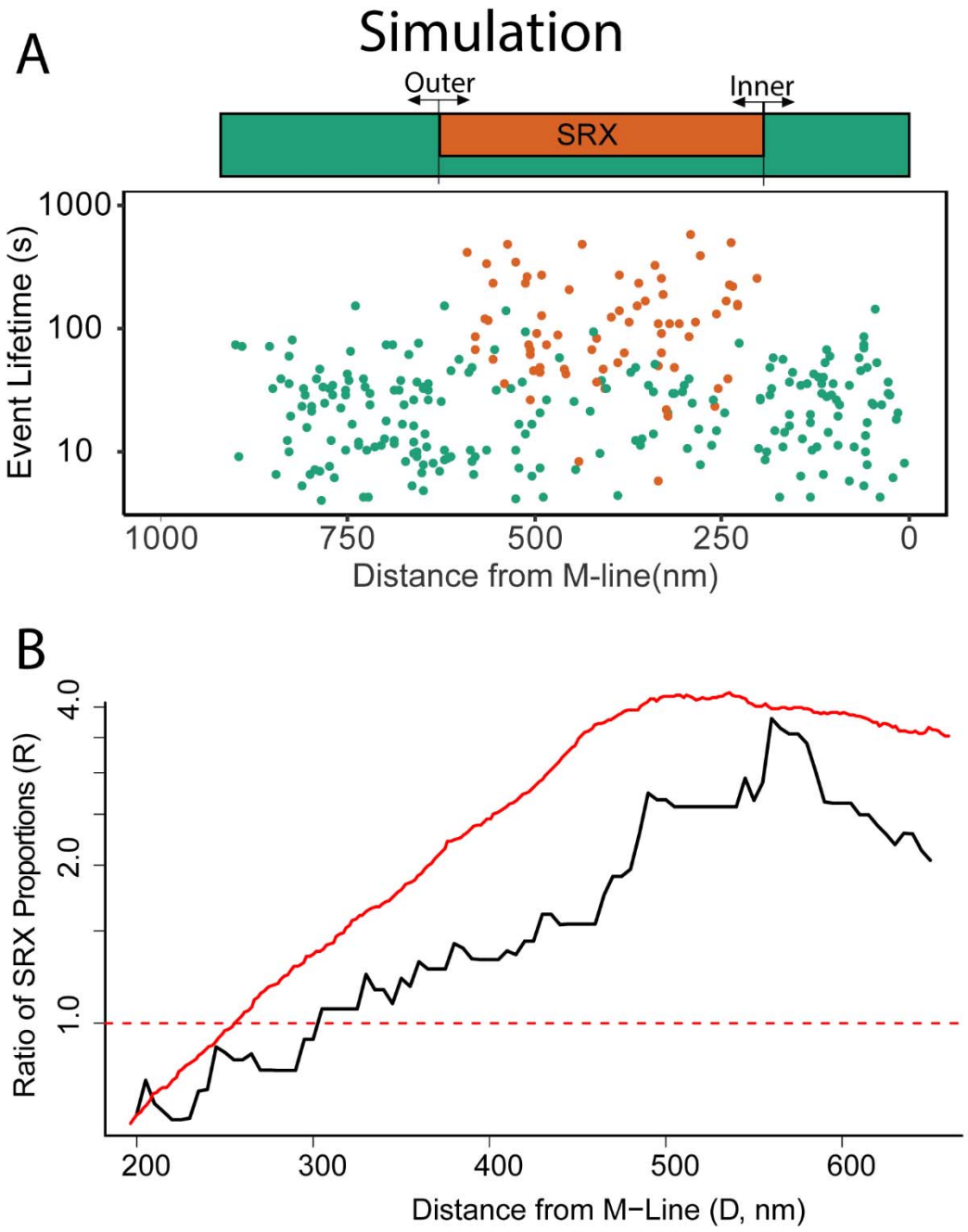

Figure S2. Simulation of spatially mapped BODIPY-ATP binding events. (A) Fluorescent-nucleotide binding events were assumed to be uniformly distributed along the length of the half-thick filament (green rectangle). The lifetime for each event (relaxed, green solid circles; SRX, orange solid circles) was determined as described above in Steps 2 and 3. Simulated SRX events occur only within a select region of the half-thick filament (orange box) and are always selected to represent 28% of the total events, in accordance with the experimental data. (B) Profile of R(D) for simulated (red) and experimental data (black).

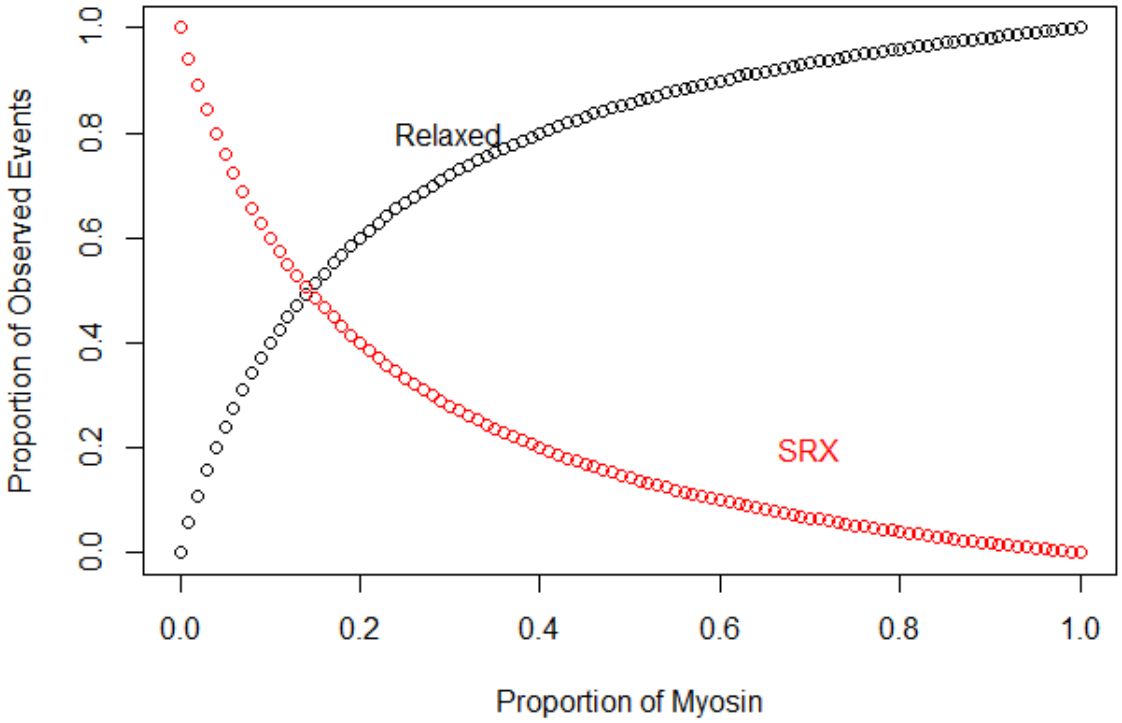

Figure S3. Predicted Relaxed/SRX proportion of observed fluorescent BODIPY-ATP binding events as a function of underlying myosin population.

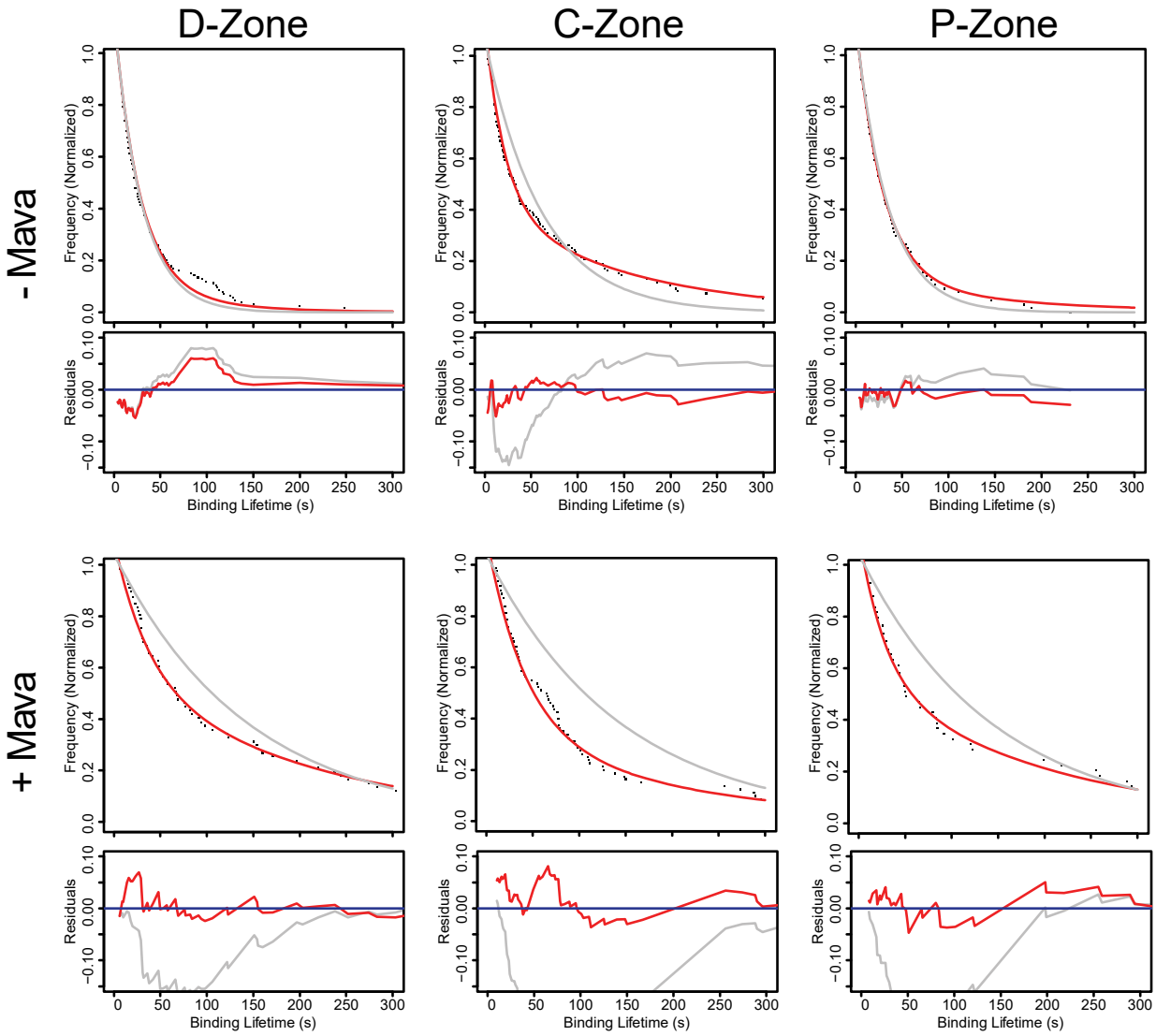

Figure S4. Survival plots of D-, C-, and P-zone fluorescent-nucleotide binding event lifetimes with (+Mava) and without Mavacamten (-Mava) as presented in Main Text Figure 3D&E. Lifetimes within each zone are fit with a single (grey line) or double (red lines) exponential function. Residuals are shown below each plot, with matching colors.

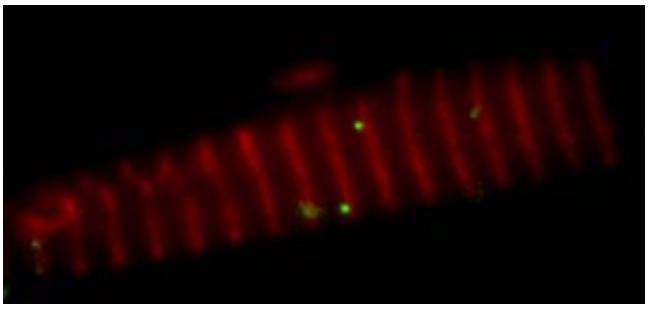

Movie S1. Fluorescent ATP binding to myofibril. Rat soleus myofibrils, labeled with anti-myomesin antibodies (red), incubated in Relaxing Buffer (see Materials and Methods). Transient binding of single molecules of BODIPY-ATP (green transient spots) are visible. Video is of 5 minutes of observation, playback is 30X real-time. Field of view measures 32 x 15 microns.